Mesoscale Modeling of Bimodal Elastomer Networks: Constitutive and Optical Theories and Results

P. R. von Lockette,*,† E. M. Arruda,‡ and Y. Wang§

Mechanical Engineering Department, Rowan University, 132 Rowan Hall, 201 Mulica Hill Road, Glassboro, New Jersey 08028; Mechanical Engineering and Macromolecular Science and Engineering, University of Michigan, Ann Arbor, Michigan 48104

ABSTRACT: A new micromechanics-based constitutive model for the nonlinear large deformation stress and birefringence responses of bimodal elastomer networks is developed. The elastic constitutive law is derived using the analytical rubrics of composite mechanics, which results in a straightforward implementation in contrast to previous bimodal theories. The model requires fewer adjustable parameters than most existing theories and, given a single set of parameters, is predictive over a wide range of bimodal compositions. Nonaffine deformation of short vs long chains is achieved with the model by satisfying equilibrium, compatibility, and the chain constitutive laws during deformation. The model is shown to agree well with data in the literature for both tensile stress and tensile stress−optic tests on specimens of poly(dimethylsiloxane) (PDMS) cross-linked from linear starting oligomers of various molecular weights. Several mixtures of eight different molecular weight combinations were examined. The model is also examined against our own data on PDMS in uniaxial compression and was shown to also predict that series of data well. Deviations of the model from the literature data are seen in bimodal mixtures which form microstructures that are believed to deviate from the proposed microcomposite arrangement. The model provides a framework for generating a constitutive theory capable of incorporating microstructural changes based solely on changes in composition.

1. Introduction

The advantages of bimodal materials have been cataloged by Mark and others who have shown that ultimate strength and toughness values find a maximum at intermediate molar concentrations of the constituents in bimodal poly(dimethylsiloxane) (PDMS) materials.[1,2] These are not the only interesting phenomena that have been found in conjunction with bimodal elastomers. Mark and Galiatsatos found a nonlinear stress−optic response in bimodal poly(dimethylsiloxane) (PDMS) through birefringence experiments[3−5] while Monnerie et al. have found that the orientation−stretch response curves of bimodal materials increase with molar percentage of short chains.[6−8] Though these phenomena have been known for some time and have been assumed to be a result of changing network structure with short chain molar percentage, a link between network microstructure and constitutive and stress−optic models has not been achieved.

Previous bimodal constitutive models have centered around the use of realistic radial distributions of the short chains in the network. A radial distribution function $W(r)$ gives the probability of finding a network chain with the end-to-end vector distance r within the network. The emphasis on generating better than Gaussian short chain distributions stems from early realizations that bimodal networks exhibit decidedly non-Gaussian behavior and therefore require non-Gaussian descriptions. The deformation behavior is assumed to result from the interaction between the stiff short chains that deform into the non-Gaussian regime and the more compliant long chains whose deformations remain Gaussian.

Derivation of the force stretch relationship for rubbery elastic materials from a known radial distribution function requires two steps. First, the free energy of all chains in the network is calculated from

$$A = -\bar{\kappa}\Theta \ln [W(r)] \tag{1}$$

where Θ is the absolute temperature and $\bar{\kappa}$ is Boltzmann's constant. Next, the force vs stretch response of the network is determined from the variation of eq 1

$$\mathscr{F} = \frac{d\Delta A}{d\lambda} \tag{2}$$

where λ is a measure of the applied macroscopic stretch and temperature is assumed to be constant. Macroscopic deformation of the network (λ) is related to local deformation of the radial distribution function ($W(r)$) through the use of analytical network averaging techniques. For example, assuming Gaussian phantomlike network behavior and tetrafunctional junctions, Erman and Mark employ[9]

$$\frac{1}{\nu}\sum_{\nu}\frac{r^2}{\langle r_0^2\rangle} = \frac{1}{3}\left[\frac{1}{2}(\lambda_x^2 + \lambda_y^2 + \lambda_z^2) + \frac{3}{2}\right] \tag{3}$$

where $\sum_{\nu}$ sums over all ν chains, λ_k is the stretch in the kth macroscopic direction, and $\langle r_0^2\rangle$ is the known second moment of the undeformed chain length averaged over all chains. In eq 3, the level of macroscopic deformation in the material as measured by λ_x, λ_y, and λ_z is related to the average change in end-to-end chain length as

* Corresponding author.
† Rowan University.
‡ Mechanical Engineering, University of Michigan.
§ Macromolecular Science and Engineering, University of Michigan.

described by $r/\langle r_0 \rangle$. The quantity $r/\langle r_0 \rangle$ is employed in the analytical description of radial distribution functions. Non-Gaussian deformations require higher order moments of $r/\langle r_0 \rangle$ than that used in eq 3, making analytical expressions typically much more complicated. Other methods employ additional computational minimization of the free energy associated with $W(r)$ in order to relate macroscopic stretch to the local stretch; see, for example, Stepto and Taylor.[10]

Initial attempts at generating bimodal theories based on the averaging techniques used in the phantom model and the constrained junction model lacked non-Gaussian behavior.[9,11] More recent bimodal constitutive theories based upon three-chain averaging[12] and phantom models[9,13] similar to eq 3 have incorporated non-Gaussian behavior by generating realistic short chain radial distributions either through analytical functions such as the Fixman–Alben distribution[9] or through the rotational isomeric states (RIS) methodology.[12,13] RIS methods provide computer-generated statistical distributions of chain conformations in order to determine a distribution function for the overall end-to-end length of a given chain based on its particular chemical structure. These realistic distributions utilize the higher moments of $r/\langle r_0 \rangle$ for the short chains. In these models long chains are assumed to deform in the Gaussian regime.

Two of the models[12,13] require involved numerical iteration schemes in order to determine six or more material parameters by curve fitting to several sets of data and further solution of nonlinear equations to generate the component stress–stretch response. The third[9] requires the determination of five material parameters by curve fitting and the solution of a nonlinear equation at each stretch increment to generate stress–stretch results. These models were developed to match experimental stress–stretch data, as can be taken from an entire mole fraction spectrum of bimodal samples, but not to *predict* the stress–stretch response of a sample of arbitrary composition. The parameters used in each of these models are taken from best fits of all stress–stretch curves available.

It should also be stressed that important micromechanics of network behavior are not accurately accounted for in these models. For example, short chain length radial distributions have been generated for chains essentially in under Θ conditions; i.e., the molecular chains are assumed to take on conformations uninhibited by other chains and without regard for the constraints that would arise from a physically cross-linked structure. Perhaps more importantly, force equilibrium at the cross-link points, where presumably long chains and short chains will meet, is not considered. Force equilibrium must be addressed since long chains and short chains, regardless of the constitutive framework or radial distributions used, will follow different force–stretch laws as seen in Figure 1. The responses shown qualitatively follow entropic descriptions of the force in a chain in terms of the number of conformational states available to the chain at a given end-to-end length or stretch λ. The value f_0 denotes the force required to achieve a zero end-to-end vector distance. Entropic considerations predict $f_0 = 0$. Figure 1 illustrates that for the same amount of external force f^* the stretch in the long chains will be more than the stretch in the short chains. Conversely, for a given amount of chain stretch, the force required to achieve
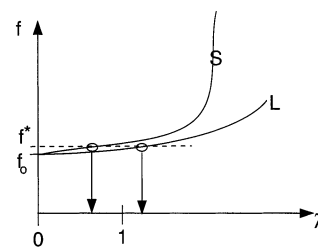
Figure 1. Sketch of expected force–stretch curves for long (L) and short (S) chains.

that deformation is larger for short chains than for longer chains. The figure also emphasizes the importance of the locking stretch as the short chain force vs stretch curve rises rapidly in a stretch regime near its limiting extensibility or locking stretch. The long chains can stretch substantially more prior to locking. The differences in the force stretch responses of the two constituents are believed to be responsible for the behavior seen in bimodal materials.

The bimodal network theory of Llorente[13] comes closest in addressing force equilibrium by using force equilibrium constraints to decompose the macroscopic stretch into its long-chain and short-chain components but this is done only after the analytical stretch-stress curve has been generated. The macroscopic deformation in bimodal theories is also often partitioned between the constituent chains in a nonphysical way through strict number or volume averaging. It is well-known in the composite mechanics community that these two approaches provide lower and upper bounds, both of which can be quite far from the actual solution.

The physical orientation behavior of bimodal networks has been addressed by analyzing regular, Gaussian, treelike phantom bimodal networks.[7,14] The orientation models derived are also limited by several assumptions. The analysis techniques used necessitate that all cross-link points must contain the same integer number of long and short chains which precludes accommodation of bimodal mixtures of arbitrary mole fraction. The deformations are restricted to the Gaussian regime even though bimodal materials have exhibited non-Gaussian behavior. [3–5] No direct kinetic interaction exists between the long and short chains; i.e., again equilibrium at junctions is not preserved during deformation. Finally, the analytical solutions generated are valid only for perfectly regular treelike networks. This precludes the occurrence of loops and larger macrocyclics known to occur in bimodal PDMS. The importance of these topologies in predicting bimodal mixtures with enhanced toughness has been shown in computational gelation simulations performed by the authors and detailed elsewhere.[15] The simulated bimodal mixtures in which increased populations of single and double cyclics were found correlated well with bimodal mixtures at which enhanced properties were seen experimentally. Increased populations of macrocyclics have also been linked to increases in the mechanical properties of interpenetrating networks.[16] Current orientation models for bimodal materials have not yet been used to generate constitutive theories of bimodal network birefringence vs stretch.

In the following section, a framework is proposed for a constitutive model to account for the changing initial morphologies of various molecular weight combinations and mole percentages of short chains in bimodal networks. Model predictions are compared to tensile stretch

data for materials having ideal bimodal molecular weight distributions with $M_s = 780–1500$ and $M_l = 17\,800–28000$. By incorporating effects of force equilibrium and compatibility directly into the model, lengthy iterative solutions and cumbersome post-solution decompositions of the deformation are avoided. To predict both birefringence vs stretch and stress vs stretch responses for an entire mole fraction spectrum of bimodal materials, the model requires only one optical and four mechanical parameters which may be found using stress–stretch and birefringence–stretch data taken from two samples of arbitrary composition. Non-affine deformation of the short and long chains is a consequence of satisfying equilibrium, compatibility and the short and long chain constitutive laws with this approach. As Mark recently surmised, this constant reapportioning of stretch between the short and long chain constituents allows intermediate bimodal blends to exhibit the synergistic response of high initial modulus and high extensibility.[17]

Physical entanglements have been shown to play a role in the behavior of networks of long chain molecules.[11,16] The bimodal networks that show enhanced and/or nonlinear behavior, however, are dominated by populations of short chains, having in excess of 90% short chains by mole. These short chains are well below the entanglement length of PDMS.[24] Simulations have also shown that unrealistic numbers of entanglements, more than would occur in the bimodal systems of interest, are required to reproduce trends in experimental results.[16] It is clear that entanglements are important network features, but their importance to the networks of interest appears minimal. Consequently, entanglements are not considered in this version of the constitutive theory.

2. Constitutive Model for Bimodal Networks

2.1. Motivation. A bimodal network is considered one in which starting oligomers (containing the same molecular moiety) of two distinct monodisperse molecular weights (generally termed long and short) are end-linked using some cross-linking agent. This presupposition is realistic owing to the particular chemistry involved in the hydrosilylation reactions used to generate PDMS networks.

Though the structures of real elastomer networks, bimodal as well as unimodal, are very complex, some similarities and differences of each type seem logical. Each chain in a unimodal network with adequate lack of polydispersity has roughly the same contour length; in an ideal case, unimodal networks will have equal molecular weights between cross-links and correspondingly equal initial chain lengths. Chain force–stretch relationships can be employed to generate force equilibrium constraint equations between chains connected at cross-links; these force equilibrium constraints must hold for all chains throughout the entire network. The network formation process for ideally unimodal elastomers may also be assumed random enough to create a spatially homogeneous structure. Hagn et al. have performed cross-linking simulations on unimodal PDMS that show that the cross-linking process produces a spatially homogeneous network structure.[18] The uniform behavior and spatial homogeneity of unimodal networks together support the author's assertion that the chains in unimodal networks will also show uniform macroscopic-to-microscopic (bulk-level to chain-level)

stretch partitoining. The effect of defects such as loops and dangling ends on equilibrium may be accounted for on a global scale by reductions in the number of active chains and need not be addressed on a discrete junction-by-junction basis.

Unlike unimodal networks, bimodal networks will not have uniform initial chain lengths nor will they have equal molecular weights between cross-links. Differences in initial chain lengths between long and short chains have been seen in simulations of bimodal networks[19] and are consistent with the proscribed bimodal distribution of molecular weights. Further evidence of heterogeneity in bimodal elastomers has been found through light-scattering experiments[20,21] and simulations of network annealing,[19] both of which show regions of short chain agglomeration in certain bimodal samples. The notion of force equilibrium, however, is still arguable in that the entire network consisting of both types of chains must remain in equilibrium for stability. Obviously, short and long chains will have different force–stretch responses (see Figure 1). Therefore, the bimodal network must have different macroscopic-to-microscopic stretch relationships for each constituent in order to remain in force equilibrium as it deforms.

Changes in network morphology are also thought to occur in both unimodal and bimodal systems as molecular weight characteristics and mixture ratios are varied. Simulations performed by the authors have shown evidence of naturally occurring reinforcement mechanisms in certain bimodal mixtures.[15] Further simulations performed by the authors have shown that changes in the chain length distributions of both the long and short chains occur while varying the same molecular weight and mixture ratio characteristics.[19] Information gained from these simulations will be incorporated into the model in a subsequent publication.

Our modeling approach first separately examines long and short chains within the network assuming each is governed by the freely jointed chain model.[22] All long chains are assumed to have the same initial length, the same amount of deformation per unit applied macroscopic deformation, and the same constitutive law. All short chains are assumed to behave similarly; however, the short chain constitutive law has different molecular parameters, and short chains will deform more or less than long chains for any given value of macroscopic deformation. The individual long and short chains are linked together, in a functional arrangement, to form a single "bimodal chain". Constraints are placed on the force and stretch of the bimodal chain to relate the force and stretch of the entire chain to that of its long and short constituents by satisfying compatibility and equilibrium. The bimodal chains are arranged in a fully three-dimensional representation of an actual network to approximate the interactions of multiple bimodal chains. The network stress response is determined from analysis of the entropy state of the deformed representative network; the birefringence response is determined from the contributions of all the deformed chains to the polarizability of the representative network.

2.2. Force Response. The individual long and short chains in the network are each modeled separately according to the freely jointed chain model which assumes that a progression of randomly oriented rigid links of length d comprise an entire network chain.[22] Assuming non-Gaussian Langevin statistics for the distribution of end-to-end vector lengths, the force in a
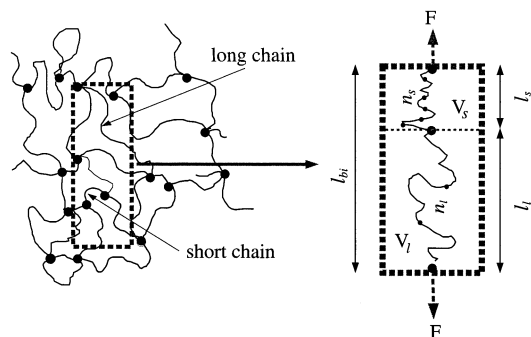
Figure 2. Given volume of amorphous bimodal network, left. Schematic of a representative bimodal chain, right. Dark circles represent chemical cross-link points.

single chain is given as

$$\mathcal{F} = \frac{\bar{\kappa}\Theta}{d}\mathcal{L}^{-1}\left(\frac{r}{r_{\max}}\right) \tag{4}$$

where d is the length of a rigid link, r is the current end-to-end vector length of the chain, and $r_{\max} = Nd$ is the maximum attainable end-to-end chain vector length before failure in which N is the number of rigid links (Kuhn steps) per segment. The Langevin function is defined as

$$\mathcal{L}(\beta) = \coth\beta - \frac{1}{\beta} \tag{5}$$

and its inverse is $\beta = \mathcal{L}^{-1}(r/r_{\max})$. Substituting $r = l_{k_0}\lambda_k$, where λ_k is the chain stretch and l_{k_0} is the initial chain length, for r in eq 4, and assuming a root mean-square (rms) approximation to the initial chain length of type k, $l_{k_0} = \sqrt{N_k}d_k$, yields the force in a chain as

$$\mathcal{F}_k = \frac{\bar{\kappa}\Theta}{d_k}\mathcal{L}^{-1}\left(\frac{\lambda_k}{\sqrt{N_k}}\right) \tag{6}$$

in which the subscript k denotes values for the given chain type k = short, long. The number of rigid links in a chain and the length of the rigid link, both of type k, become N_k and d_k, respectively.

2.3. Kinematic Constraints. Schematic representations of a bimodal network are shown in Figure 2. The figure shows long and short chains cross-linked together in a random arrangement on the left while the right shows a schematic of a representative bimodal chain. In the schematic on the right, long chains (in the lower portion) and short chains (in the upper portion) are shown linked end-to-end, creating a long chain segment and a short chain segment of the bimodal chain. As shown in the figure, the long and short chain segments have lengths l_l and l_s, respectively. V_k is the volume fraction of k-type material in the model. The relationships $l_{bi} = l_l + l_s$ and $V_s + V_l = 1$ hold. The number of individual long and short chains occupying the representative volume is dependent on the concentrations and molecular weights of each of the constituents. The number density of phase k, ϕ_k, can be found from

$$\phi_k = \frac{n_k m_k M_k}{\rho} \tag{7}$$

when mole fractions are given or from

$$\phi_k = n_k V_k \tag{8}$$

when volume fractions are known. M_k is the molecular weight, m_k is the mole fraction, n_k is the number density of a unimodal sample, and V_k is the volume fraction of the k-type material present in the bimodal specimen; ρ is the mass density of the bimodal mixture. Negligible variation in the mass densities of various molecular weight unimodal samples and various molecular weight combinations in bimodal samples makes use of $\rho = \rho_s = \rho_l$ in eq 7, a reasonable assumption.

Series and parallel arrangements are two natural configurations which follow from the rubrics of the anlaysis of composite media. The individual long and short chains in the bimodal chain are assumed to exist in series within the volume element for several reasons. Simulations have shown that parallel arrangements of chains between pairs of cross-links very rarely occur.[15] In simulations of bimodal materials corresponding to the materials studied here, parallel arrangements of long chains did not occur with any statistical significance. Significant numbers of parallel arrangements between pairs of cross-links were formed only by short chains. Furthermore, though the percentages of parallel arrangements varied with bimodal composition, the highest percentage of cross-link connections made by two or more chains was only 6% for all compositions studied.[15]

In addition to parallel arrangements composed of two chains connecting a pair of cross-links, there are an infinite number of parallel paths between any pair of cross-links when a path is allowed to traverse any number of chains in series. In this case paths between cross-links must pass through several *other* cross-links before reaching either of the original pair of cross-links in question. For large parallel structures, as more cross-links are incorporated into the path between two given cross-links the force−stretch response between the original pair of cross-links is increasingly affected by the response of the network. In this analysis, the authors incorporate network effects through use of the eight-chain network averaging approach discussed in the following section. The series arrangement used to describe the material at the chain level accounts for the primary mode of connection between cross-links, i.e., individual chains connecting pairs of cross-links. Together, the series arrangement and network averaging methods provide a model that incorporates the effects of the primary mode of cross-link connectivity as well as the network effects of larger parallel arragenments.

Force equilibrium of the serial bimodal chain requires that the force in a single short chain equals the force in a single long chain. From eq 6 this constraint reduces to

$$\frac{\lambda_l}{\lambda_s} = \sqrt{\frac{N_l}{N_s}} \tag{9}$$

in which d_l/d_s is assumed to be unity, giving the long and short chains equivalent persistence lengths since the persistence length is equivalent to the length of the rigid link in the freely jointed chain model. This resulting kinematic constraint ensures that each of the chains is at the same fraction of its limiting extensibility. It also provides for enormous differences in the long and short chain stretches which may or may not be realistic.
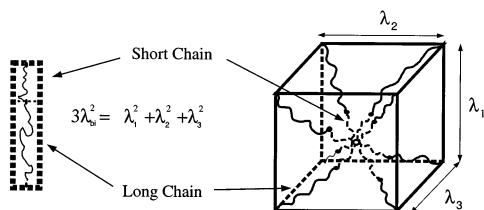
Figure 3. Bimodal chains are arranged into the eight-chain framework to generate the complete network theory. The cube deforms affinely as its sides remain parallel to the principal deformation directions. The stretches in the constituents, given in eq 12, are nonaffine.

Instead of using the rms assumption which leads to eq 6, initial lengths of each type of chain are given by a scaled rms assumption, $l_{k_o} = \Psi_k \sqrt{N_k} d_k$. Scaling is required to account for steric constraints, intermolecular effects, and network morphology[19] which alter the unperturbed lengths of long chains and short chains from their rms lengths. Current chain lengths are given in terms of the chain stretch and original lengths as $l_k = l_{k_o}\lambda_k$. The bimodal chain length is determined by summing the lengths of all short and long chains within the volume element. Defining the stretch in the entire bimodal chain as

$$\lambda_{bi} = \frac{l_{bi}}{l_{bi_o}} = \frac{\phi_s l_s + \phi_l l_l}{\phi_s l_{s_o} + \phi_l l_{l_o}} \tag{10}$$

leads to the geometric compatibility requirement,

$$\lambda_{bi} = \frac{\Psi_s n_s V_s \sqrt{N_s} \lambda_s + \Psi_l n_l V_l \sqrt{N_l} \lambda_l}{\Psi_s n_s V_s \sqrt{N_s} + \Psi_l n_l V_l \sqrt{N_l}} \tag{11}$$

This reduces to

$$\lambda_{bi} = \frac{\lambda_s + \dfrac{\Psi_l}{\Psi_s}\mathscr{A}\lambda_l}{1 + \dfrac{\Psi_l}{\Psi_s}\mathscr{A}}; \quad \mathscr{A} = \frac{n_l V_l \sqrt{N_l}}{n_s V_s \sqrt{N_s}}, \tag{12}$$

a relationship between stretch in the bimodal chain and the stretch in its long and short constituents. This also highlights the effects of material composition on the contributions of each component to the overall stretch via the factor $\mathscr{A}$. As the volume, or number, of short chains in the system increases $\mathscr{A} \to 0$ forcing a short-chain-stretch dominated system. Conversely, as the number, or volume, of the long chains in the system increases, $\mathscr{A} \to \infty$ forcing a system characterized by the stretch of the long chains. Equation 12 depends nonlinearly on material composition via $\mathscr{A}$; small changes in molar composition can cause large changes in volume fractions and thus in $\mathscr{A}$. The ratio of the initial chain lengths is also shown to be important and to have a similar effect on the bimodal chain stretch.

3. Network Averaging

Bimodal chains subject to their internal equilibrium and compatibility constraints given by eqs 9 and 12, are arranged in a contraction of a real network in Figure 3 to model the fully three-dimensional response of the entire bimodal network. This unit cell network uses eight spars, each consisting of a bimodal chain, which radiate outward from the center to the vertexes of a unit

cube. The edges of the cube are assumed to be parallel to the principal axes of stretch. The vertexes of the cube are also assumed to move affinely with macroscopic deformation leading to the following relation between the principal stretches and the stretch in a bimodal chain along any spar $\lambda_{bi} = (1/\sqrt{3})\sqrt{\lambda_1^2 + \lambda_2^2 + \lambda_3^2}$. This arrangement of chains is identical to that used in the eight-chain model[23] for random elastomeric materials in which a distribution of chain lengths was assumed to be modeled in terms of an average chain of length N and network density n. Please see the reference[23] for additional details and experimental validation of the eight-chain model.

In the bimodal network theory, affine deformation of the unit cube will produce affine deformation of a composite bimodal chain but does not produce affine deformation of a bimodal chain's short and long constituents. The apportioning of stretch within the bimodal chain depends on both the macroscopic stretch and on the composition of the bimodal network and is given in eq 12; therefore, the bimodal chain theory is a nonaffine constitutive law.

4. Stress Response of the Bimodal Network

Stress response of the bimodal chain model is found from examining the contribution of each of the individual bimodal chains to the total entropy as the unit cell network responds to macroscopic deformation. An expression for the total entropy is used to calculate a strain energy function, which in turn is used to determine an expression for the stress. The entropy in a single chain is given by[25]

$$s_k = c - \bar{\kappa} N_k \left(\frac{r_k}{N_k d_k} \beta_k + \ln\frac{\beta_k}{\sinh \beta_k} \right); \quad \beta_k = \mathscr{L}^{-1}\left(\frac{r_k}{r_{max_k}} \right) \tag{13}$$

where c is a constant. Summing the entropy contributions of all the long and short chains in the network gives the total network entropy as

$$S_{bi} = n_s V_s s_s + n_l V_l s_l \tag{14}$$

The strain energy of the network, W, follows from the entropy as

$$W = -\Theta(S_{bi} - S_{bi_o}) \tag{15}$$

where S_{bi_o} is the initial entropic state of the unstretched network. In eq 15, internal energy changes are neglected. The stress in the bimodal model is found from the work-energy relationship assuming incompressibility ($\lambda_1 \lambda_2 \lambda_3 = 1$)

$$\sigma_i - \sigma_j = \frac{dW}{d\lambda_i}\lambda_i - \frac{dW}{d\lambda_j}\lambda_j \tag{16}$$

Applying the chain rule to eq 16 yields

$$\sigma_i - \sigma_j = \left(\frac{dS_{bi}}{d\lambda_s}\frac{d\lambda_s}{d\lambda_{bi}} + \frac{dS_{bi}}{d\lambda_l}\frac{d\lambda_l}{d\lambda_{bi}} \right)\left(\lambda_i\frac{d\lambda_{bi}}{d\lambda_i} - \lambda_j\frac{d\lambda_{bi}}{d\lambda_j} \right)\Theta \tag{17}$$

The stress vs stretch relationship is determined from eqs 12−17 to be

$$\sigma_i - \sigma_j = \frac{\bar{\kappa}\Theta}{3}\left(\frac{1 + \mathscr{A}}{1 + \mathscr{A}\sqrt{\dfrac{N_l}{N_s}}}\right)\left(n_s V_s \sqrt{N_s} + \right.$$

$$\left. n_l V_l \sqrt{N_l}\sqrt{\frac{N_l}{N_s}}\mathscr{L}^{-1}\left(\frac{\bar{\Psi}\bar{\lambda}}{\sqrt{\bar{N}}}\right)\left(\frac{\lambda_i^2 - \lambda_j^2}{\lambda_{bi}}\right)\right) \quad (18)$$

where from eq 6 and the scaled rms assumption, the equilibrium condition

$$\frac{\bar{\Psi}\bar{\lambda}}{\sqrt{\bar{N}}} = \frac{\Psi_s \lambda_s}{\sqrt{N_s}} = \frac{\Psi_l \lambda_l}{\sqrt{N_l}} \quad (19)$$

must hold. The principal stress difference is given in eq 18; absolute values of principal stresses require the boundary conditions associated with a given deformation state.

5. Birefringence Response of the Bimodal Network

Polarizability, and therefore birefringence, is a direction dependent, tensor quantity. Each chain in the network makes a contribution to the total value based upon its stretch as well as its relative "inclination" (used to avoid confusion with "orientation") to some reference set of axes. In both the unimodal eight-chain and the bimodal chain models, the set of principal axes is this reference set. The unimodal eight-chain model and the long and short components of the bimodal chain model also have the same chain inclinations, respectively, due to the series arrangement. The result is an expression similar to the eight-chain model birefringence[26]

$$\Delta h_{i-j} = \left(\frac{2\pi(\eta_0^2 + 2)^2}{9}\frac{}{\eta_0}\right)\left(\frac{\alpha(n_s N_s V_s + n_l N_l V_l)}{3}\right)$$
$$\left(1 - \frac{\dfrac{3\Psi\bar{\lambda}}{\sqrt{\bar{N}}}}{\mathscr{L}^{-1}\left(\dfrac{\bar{\Psi}\bar{\lambda}}{\sqrt{\bar{N}}}\right)}\right)\left(\frac{\lambda_i^2 - \lambda_j^2}{\lambda_{bi}^2}\right) \quad (20)$$

in which η_0 and α are the mean refractive index of the material and polarizability anisotropy of a rigid link, respectively. The eight-chain arrangement was proven highly effective by the authors in predicting the Raman scattering response (a fourth order measure of the complete polarizability tensor) for amorphous PET and in predicting the nonlinear optical state during large shear deformation tests on PDMS.[27] The expression for birefringence in eq 20 differs from the eight-chain birefringence in its direct incorporation of the effects of having bimodal constituents, namely in the short and long contributions to the second term of eq 20. Decomposition of the nonaffine deformation of the long and short chains is also incorporated in eq 20 through the compatibility condition of eq 12.

6. Comparison with Experimental Results

In this section, the model is compared to experimental data in the literature on various bimodal PDMS specimens.[1,2,5] These experimental results are under uniaxial tension. The model is also compared to our own data on bimodal PDMS conducted in uniaxial compression.

6.1. Model Constant Definition. The bimodal network model has six mechanical and one optical parameters, Ψ_s, Ψ_l, N_s, N_l, n_s, n_l, and α. In theory, only Ψ_s

and Ψ_l are adjustable for a given bimodal network. The number of parameters can be reduced by two by examining extremum concentration cases in uniaxial deformation. By constructing the ratios of initial stress−stretch and either the birefringence−stretch or birefringence-stress predictions for the extremum unimodal cases and making small strain (Gaussian) approximations on the Langevin function, one can draw relationships among the chain density, number of links per chain for each constituent, and the rms scaling factors. The ratio of initial stress−stretch slopes for purely unimodal materials in tension yields

$$\frac{\sigma_l}{\sigma_s} = \frac{n_l}{n_s}\left(\frac{\Psi_l}{\Psi_s}\right) \quad (21)$$

where σ_k is the stress in a material of type k resulting from a small applied stretch. The ratio of initial birefringence−stretch slopes for purely unimodal materials yields

$$\frac{\Delta\eta_l}{\Delta\eta_s} = \frac{n_l}{n_s}\left(\frac{\Psi_l}{\Psi_s}\right)^2 \quad (22)$$

where $\Delta\eta_k$ is the birefringence of a unimodal sample of type k resulting from a small applied stretch. Equations 21 and 22 yield the ratio of the initial stress optic coefficients

$$\frac{C_l}{C_s} = \left(\frac{\Psi_l}{\Psi_s}\right) \quad (23)$$

where C_k is the stress−optic coefficient of a unimodal sample of material k in the Gaussian regime. Forcing the ratios to fit experimental data for unimodal long and unimodal short chains reduces the number of independent parameters by two. This same technique can be applied to cases where only data on interim concentrations are available. The number of independent parameters is still reduced by two, though the relationships between parameters are not as simple. The model has the distinct advantage over other bimodal constitutive theories in that it does not require detailed sets of data over the complete molar spectrum of a given bimodal combination to determine the model parameters. Parameters may be chosen from bests fits of two concentrations and then used to predict the response of arbitrary molar mixtures. In addition, the model does not require solution of supporting equations in the generation of stretch-stress results or in the determination of the behavior of the long and short chain components.

6.2. Stress−Optic Response. Figures 4−6 show the normalized initial stress−optic coefficients as functions of short chain content by volume from uniaxial tensile tests[5] on the three bimodal PDMS systems given in Table 1. Stress−optic coefficient values are normalized to their unimodal long case. Experimental results are given by symbols; analytical results using eqs 18 and 20 in the Gaussian range are shown by solid lines. Dashed and dotted lines represent volume and molar rules of mixtures approximations, respectively, derived from best fits of the standard eight-chain model[23,26] for each extremum unimodal case; these curves are calculated using $C = C_s V_s + C_l V_l$ for volume rule of mixtures or $C = C_s m_s + C_l m_l$ for molar rule of mixtures.
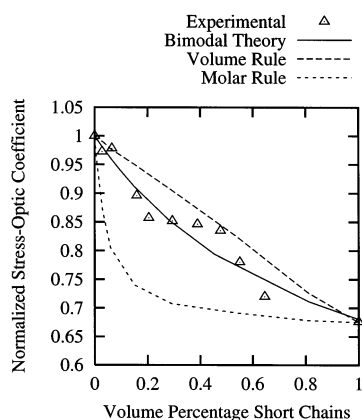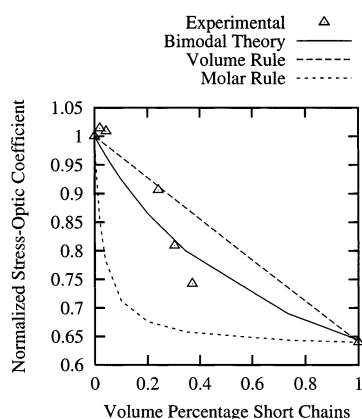
Figure 4. Stress−optic coefficient vs volume fraction for bimodal PDMS having $M_l = 17\,800$ and $M_s = 780$ found under uniaxial tension tests.[5] Symbols represent experimental data points, solid lines the bimodal network theory, dashed lines a volume rule of mixtures, and dotted lines a molar rule of mixtures.
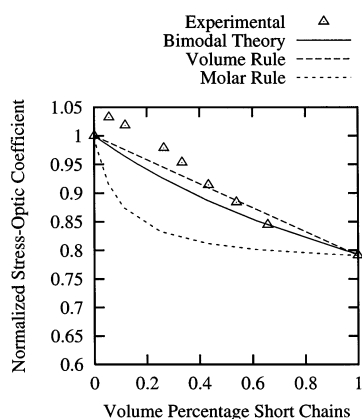
Figure 5. Stress−optic coefficient vs volume fraction for bimodal PDMS having $M_l = 17\,800$ and $M_s = 1500$ found under uniaxial tension tests.[5] Symbols represent experimental data points, solid lines the bimodal network theory, dashed lines a volume rule of mixtures, and dotted lines a molar rule of mixtures.

Figure 6. Stress−optic coefficient vs volume fraction for bimodal PDMS having $M_l = 28\,000$ and $M_s = 780$ found under uniaxial tension tests.[5] Symbols represent experimental data points, solid lines the bimodal network theory, dashed lines a volume rule of mixtures, and dotted lines a molar rule of mixtures.

Moving from one extremum case, unimodal long ($V_s = 0$), to the other, unimodal short ($V_s = 1$), in Figures 4−6, a clear reduction is seen overall in the stress−optic coefficients in each system. The ratios of the unimodal

**Table 1. Composition of Bimodal Systems for Stress−Optic Tests**

system ID	long chain mol wt	short chain mol wt
780A	17 800	780
1500	17 800	1500
780B	28 000	780

short (C_s) to unimodal long (C_l) stress−optic coefficients, C_s/C_l, are 0.67, 0.79, and 0.65 for systems 780A, 1500, and 780B, respectively. In conjunction with eq 23 these figures suggest $\Psi_s \neq \Psi_l$. This implies that the rms assumption does not hold for both the long and short chains in a bimodal system validating the assumptions leading to eq 12.

Figures 4−6 demonstrate that the stress−optic coefficients of bimodal networks are closer to the upper bound volume rule of mixtures analysis than to the lower bound analysis. At intermediate concentrations, it appears that additional factors, possibly related to network topology, are also at work in addition to the strong dependence on short chain volume. Data in Figures 5 and 6 show bimodal mixtures with larger stress−optic coefficients than either constituent. Volume mixture analysis is a rubric of composite analysis techniques whereas molar (or number) averaging schemes are not. The molar averaging schemes shown here clearly are not indicative of the stress−optic coefficient response. This is an important observation since previous bimodal constitutive theories employ mole fraction ratios when apportioning the macroscopic stretch to the long and short chain components. The bimodal network theory herein incorporates the influence of both mole fraction and volume fraction through its dependence on number density. The bimodal theory predicts the trend in C vs short chain content for all three systems studied better than either rule of mixtures assumption.

The effect of the rms scaling is an important question to be addressed later in this work and in more detail in upcoming work by the authors. Preliminary results from this other work examining networks formed using the computer algorithm NETSIM[15] show that the rms scaling varies with molecular weight combination and also with mixture composition in bimodal systems. When bimodal networks are in the macroscopically undeformed equilibrium state, short chains with given molecular weights will exist on average at different fractions of their rms lengths depending on the mixture ratios of the bimodal constituents and on the molecular weights of the long chain components. Variation in the equilibrium lengths of the chains leads to variation in the network's stress−stretch response due to the nonlinear state dependent nature of an elastomer chain's force−stretch response (see Figure 1). These results suggest that Ψ_l and Ψ_s vary with composition in bimodal networks in a manner that is as yet uncharacterized. In the upcoming discussion, $\Psi_l = \Psi_s = 1$ is examined initially for analysis purposes.

6.3. Stress−Stretch Response. Figures 7−10 depict the experimental stress vs stretch response of various bimodal PDMS specimens in uniaxial tension.[1,2] Figure 11 shows the experimental stress vs stretch response of various bimodal PDMS specimens in uniaxial compression tests conducted by the authors. Each figure represents a mole fraction family for the molecular weight combinations given in Table 2. Symbols represent experimental data points, lines represent analytical predictions from eq 18. Model parameters, which remain
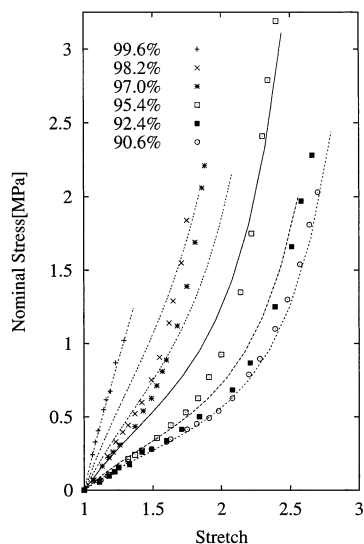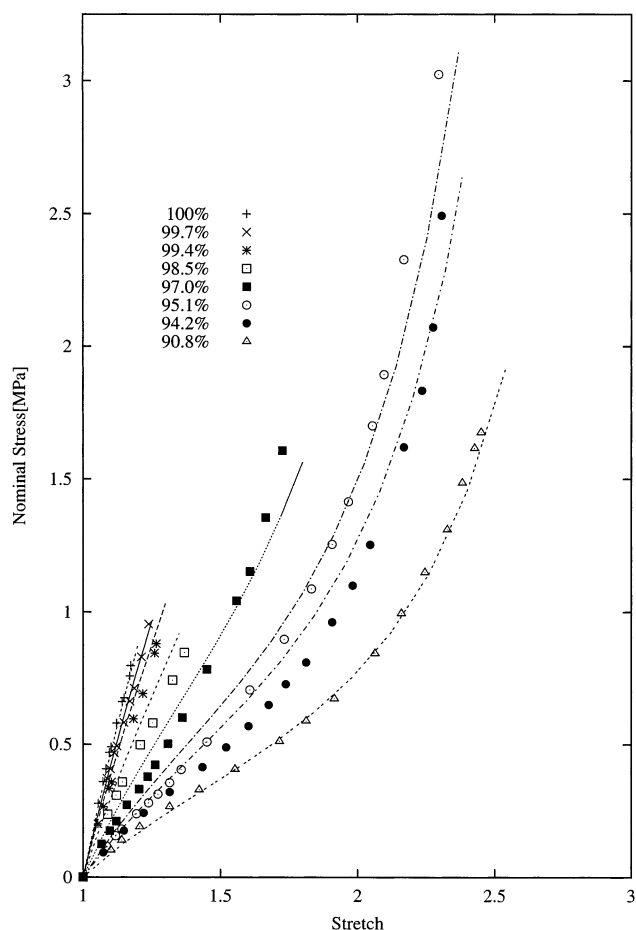
Figure 7. Stress vs stretch response for bimodal PDMS specimens having $M_l = 21\,300$, $M_s = 460$, and the molar concentrations of short chains shown found under uniaxial tension.[2] Symbols represent experimental data points and lines the bimodal network theory. Model parameters used: $N_s = 2$, $N_l = 10$, $n_s = 2.60 \times 10^{20}$ m^{-3}, $n_l = 5.00 \times 10^{18}$ m^{-3}, and $\Psi_s = \Psi_l = 1$.

fixed over the entire mole fraction range in each figure, are chosen by matching eq 21 to the experimental data and using best fits of N_s and N_l for only the extremum cases. For example, $m_s = 99.6\%$ and $m_s = 90.6\%$ are used in Figure 7. Each figure shows the ability of the model to predict stress−stretch response across the entire family of mole fractions in both tension and compression.

In Figures 7−9, the model is compared to tension data by Mark and Tang[2] in which the short chain molecular weight varies in each figure. The stress vs stretch response of these networks varies tremendously as a result of a 10 mol % change in short chain content. The response of the bimodal blends is highly nonlinear elastic whereas unimodal short networks exhibit nearly linear elastic behavior. The initial or rubbery modulus of PDMS networks depends strongly on the short chain content. The model predicts the change in stress−stretch response with mol % short chains with good accuracy, especially in the large stretch regimes, for all bimodal materials in Figures 7−9.

System 460, the system with the shortest short chain component, shows the largest deviation from the theory at intermediate mixtures even though the extremum mixtures are captured quite well. All previous bimodal theories have difficulty in capturing the stress−stretch response of bimodal mixtures with very low molecular weight short chain components, and several do not accurately capture the unimodal short case. Previous work by the authors provides evidence which suggests that as the short chain molecular weight drops, changes in network topology deviate farther from the assumed features accounted for in the bimodal theory[15] which could result in the model's deviation from the data. In particular these networks tend to have a higher incidence and proportion of stiff short chain connections and fewer overall network junctions.[15] This may result in deviations from prior assumptions of equal persistance lengths (i.e., $d_s \neq d_k$) and from a unity ratio in rms scaling factors (i.e., $\Psi_s/\Psi_l \neq 1$) used in section 2.
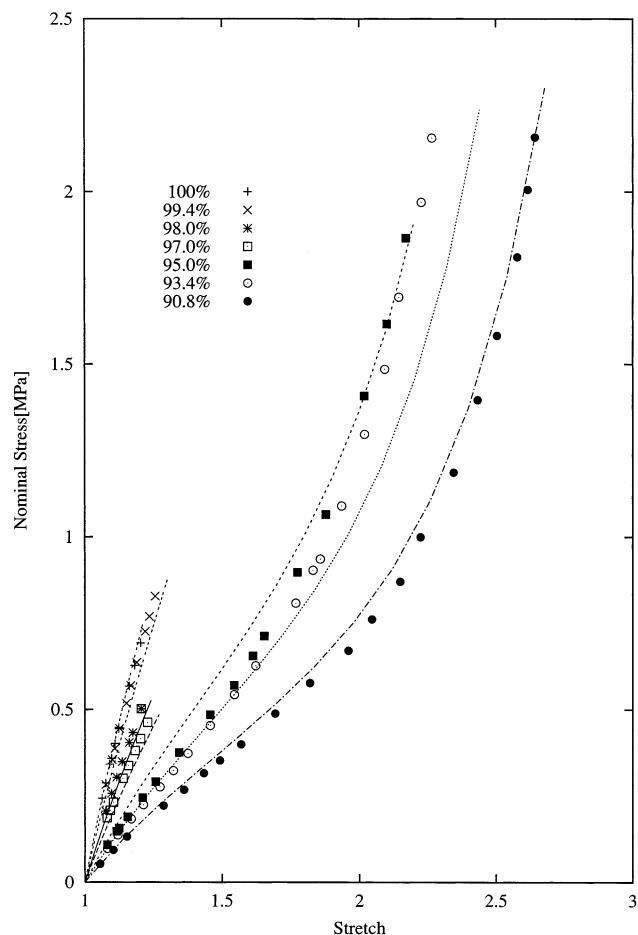

Figure 8. Stress−stretch response for bimodal PDMS specimens having $M_l = 21\,300$, $M_s = 660$, and the molar concentrations of short chains shown found under uniaxial tension tests.[2] Symbols represent experimental data points and lines the bimodal network theory. Model parameters used: $N_s = 2$, $N_l = 10$, $n_s = 2.60 \times 10^{20}$ m^{-3}, $n_l = 7.00 \times 10^{18}$ m^{-3}, and $\Psi_s = \Psi_l = 1$.

In terms of a macroscopic constitutive model, evidence hinting that the long and short chains in unimodal mixtures behave differently than their bimodal counterparts[7,8] would suggest that the bimodal model must also accommodate those changes. A first approximation was found through examination of the stress−optic results in conjunction with eq 23 that suggests $\Psi_l/\Psi_s \neq 1$ resulting in deviation from the rms assumption for initial chain lengths. This result is not surprising since it is well-known that the characteristic length of long chain molecules varies with molecular weight.

The model parameters for the system 1100, Figure 10, are determined by fixing $\Psi_s = 0.87$ and $\Psi_l = 1.10$ which yields $\Psi_s/\Psi_l = 0.79$, a value taken from sample 1500 for which stress−optic data are available, and is similar to system 1100 for which the stress−stretch response is given. The new parameters reflect the expected change in stress optic-coefficient over the range of mole fractions. The reduction in initial length of the short chain component as compared to its rms length can be seen as both a natural occurrence of changes in the characteristic ratio and a consequence of having an equilibrated network, i.e., the stiffer short chains contract forcing the more compliant long chains to extend to maintain equilibrium at the cross-links. The model with the new parameters is compared to experimental data for system 1100 in uniaxial tension[1] in Figure 10.
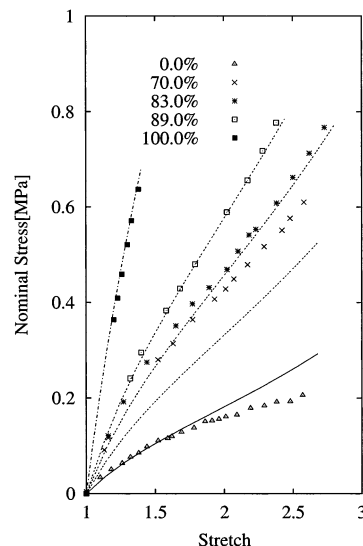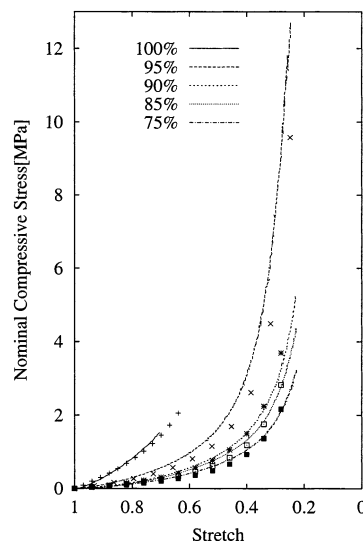
Figure 9. Stress–stretch response for bimodal PDMS having $M_l = 21\,300$, $M_s = 880$, and the molar concentrations of short chain material shown found under uniaxial tension tests.[2] Symbols represent experimental data points and lines the bimodal network theory. Model parameters used: $N_s = 2.1$, $N_l = 10$, $n_s = 2.20 \times 10^{20}$ m^{-3}, $n_l = 9.00 \times 10^{18}$ m^{-3}, and $\Psi_s = \Psi_l = 1$

Figure 10 displays the model predictions for the data of Mark[1] over a very broad range of bimodal compositions. The model fails to capture the finite stretch response of the 0 mol % short composition, but the best fit to the small and moderate stretch regimes predicts the intermediate compositions well. The figure shows that the model may accommodate deviation from the initial rms assumption and still retain its efficacy in predicting the macroscopic stress vs stretch response. The assumption of initial short chain lengths reduced below their rms values is in agreement with recent work by the authors demonstrating that annealed unimodal and bimodal networks have short chain lengths of less than 90% of their rms values.[19] The model is effective in predicting stress vs stretch while using parameters adjusted to fit the drop in the stress–optic coefficient. The adjustment for accommodation of stress–optic data makes only slight changes in the curvature of the stress–stretch response curves from use of the best-fit model with $\Psi_s = \Psi_l = 1$ (not shown).

The model accommodates the stress–optic data by requiring a shift in the short and long chain densities, n_s and n_l, in the best fit of the extremum cases. Physically, the increase in n_s represents more densely packed short chains which agrees qualitatively with a decrease in Ψ_s representing short chain contraction. Conversely, the decrease in n_l represents less densely

Figure 10. Stress vs stretch response for bimodal PDMS having $M_l = 18\,500$ and $M_s = 1100$, and the concentrations of short chains shown found under uniaxial tension tests.[1] Symbols represent experimental data points and lines the bimodal network theory. Model parameters used: $N_s = 8$, $N_l = 10$, $n_s = 2.2 \times 10^{20}$ m^{-3}, $n_l = 22 \times 10^{19}$ m^{-3}, $\Psi_s = 0.87$, and $\Psi_l = 1.1$.

Figure 11. Stress–stretch response found under uniaxial compression tests conducted by the authors for bimodal PDMS having $M_l = 21\,500$, $M_s = 780$, and the molar concentrations of short chains shown. Lines represent experimental data and symbols the bimodal network theory. Model parameters used: $N_s = 2.1$, $N_l = 10$, $n_s = 1.60 \times 10^{20}$ m^{-3}, $n_l = 2.40 \times 10^{19}$ m^{-3}, and $\Psi_s = \Psi_l = 1$.

Table 2. Composition of Bimodal Systems for Stress–Stretch Tests

system ID	long chain mol wt	short chain mol wt
460	21 300	460
660	21 300	660
780	21 500	780
880	21 300	880
1100	18 500	1100

packed long chains, which agrees qualitatively with an increase in Ψ_l representing long chain extension. Though the rms scaling factor ensures correct transitioning of the stress–optic coefficient between the extremum cases and is able to modify the curvature of the stress–stretch response curves of the network, it may not be able to

completely account for all changes in network topology as evidenced by the model's deviation from the data at finite stretch for the unimodal long case.

The model predictions are compared to PDMS data in uniaxial compression in Figure 11. These data were generated under constant strain rate conditions using small compression specimens and lubricant at speciman/platen interfaces to reduce friction and ensure homogeneous deformation. The responses at short chain molar contents of 100% and 75% were used to determine the model parameters. The model accurately predicts the intermediate responses at short chain molar contents of 95%, 90%, and 85%.

7. Conclusions

Agreement of the bimodal stress−stretch and stress−optic models to data suggests several things. First, the series arrangement of a bimodal chain is an acceptable approximation to the actual network connectivity especially when combined with eight-chain averaging of chains in the network. The configuration results in a force equilibrium constraint which solves several previous modeling issues including that of addressing kinematic equilibrium at junctions and avoiding the need for lengthy iterative solution schemes. Force equilibrium constraints resulting in eq 19 along with the ratios of unimodal experimental stress−optic results (see Figures 4−6) also necessitate $\Psi_s/\Psi_1 \neq 1$. This suggests the rms assumption may not hold even when accounting for changes in the characteristic ratio. If this is true, then it is also likely that Ψ_s and Ψ_1 must change with changes in the constituents. In addition, increasing deviation between data and model results near critical mixtures in system 460 (mixtures at or near those in which ultimate strengths and toughnesses are maximized) suggests micromechanical changes that occur with composition; the nature of these changes is further addressed in recent work by von Lockette and Arruda.[15] Work is underway by the authors to catalog changes in the initial chain lengths with composition in the bimodal network and to determine the effects of initial chain length on network load bearing mechanisms and network failure. Results of these further analyses may then be incorporated into the bimodal network framework, improving the model's accuracy for systems with high incidence of network defects.

References and Notes

(1) Mark, J. E. *Adv. Polym. Sci.* **1982**, *44*, 1−25.
(2) Mark, J. E.; Tang, M. Y. *J. Polym. Sci.: Polym. Phys. Ed.* **1984**, *22*, 1849−1855.
(3) Galiatsatos, V.; Mark, J. E. *Macromolecules* **1987**, *20*, 2631−2632.
(4) Galiatsatos, V.; Mark, J. E. In *Silicon Based Polymer Science: A Comprehensive Resource*; Zeigler, J. M., Fearon, F. W. G., Ed.; American Chemical Society: Washington, DC, 1990, pp 201−206.
(5) Galiatsatos, V.; Subramanian, P. R. *Makromol. Chem., Macromol. Symp.* **1993**, *76*, 233−240.
(6) Monnerie, L.; Besbes, S.; Ceremelli, I.; Bokobza, L. *Macromolecules* **1992**, *25*, 1949−1954.
(7) Bahar, I.; Erman, B.; Bokobza, L.; Monnerie, L. *Macromolecules* **1995**, *28*, 225−231.
(8) Monnerie, L.; Besbes, S.; Ceremelli, I.; Bokobza, L. *Macromolecules* **1995**, *28*, 231−235.
(9) Erman, B.; Mark, J. E. *J. Chem. Phys.* **1988**, *89*, 3314−3316.
(10) Stepto, R. F.; Taylor, D. J. R *J. Chem. Soc., Faraday Trans.* **1995**, *91*, 2639−2647.
(11) Higgs, P. G.; Ball, R. C. J. *J. Phys. (Paris)* **1988**, *49*, 1785.
(12) Mark, J. E.; Curro, J. G. *J. Chem. Phys.* **1983**, *79*, 5705−5709.
(13) Llorente, M. A.; Rubio, A. M.; Freire, J. J. *Macromolecules* **1984**, *17*, 2307−2315.
(14) Kloczkowski, A.; Mark, J. E.; Erman, B. *Macromolecules* **1991**, *24*, 3266−3275.
(15) von Lockette, P. R.; Arruda, E. M. *Macromolecules* **1999**, *32*, 1990−1999.
(16) Termonia, Y. *Macromolecules* **1991**, *24*, 1392−1396.
(17) Mark, J. E. *Rubber Chem. Technol.* **1999**, *72*, 465−483.
(18) Hagn, C.; Wittkop, M.; Kreitmeier, S.; Trautenberg, H. L.; Holzl, T.; Goritz, D. *Polym. Gels Networks* **1997**, *5*, 327−337.
(19) von Lockette, P. R.; Arruda, E. M. *Comput. Theor. Polym. Sci.* **2001**, in press.
(20) Soni, V. K.; Stein, R. S. *Macromolecules* **1990**, *23*, 5257−5265.
(21) Oikawa, H. *Polymer* **1992**, *33*, 1116−1119.
(22) Kuhn, W.; Grün, F. *Kolloid. Z.* **1942**, *101*, 248−271.
(23) Arruda, E. M.; Boyce, M. C. *J. Mech. Phys. Solids* **1993**, *41*, 389−412.
(24) Strobl, B. *The Physics of Polymers: Concepts for Understanding Their Structures and Behavior*, 2nd ed; Springer, New York, 1996.
(25) Treloar, L. R. G. *The Physics of Rubber Elasticity*; Oxford University Press: Oxford, England, 1975.
(26) Arruda, E. M.; Przybylo, P. A. *Polym. Eng. Sci.* **1995**, *35*, 395−402.
(27) von Lockette, P. R.; Arruda, E. M. *Acta Mech.* **1997**, *134*, 81−107.

MA000547Y